

「太陽エネルギー変換用酸化チタン半導体の研究」

Chapter 1

General Introduction

1.1 Background

Energy is the source of life and from time immemorial sun has been the source of energy. In the flow of wind, in the cascade of waves in the sea, in the movement of a living being and in the growing up of a child, energy is manifested in different forms and of which sun has been the sole source. In all times, man has looked for energy to make his life more comfortable and more active. With the gradual development of human civilization, man has learnt to extract energy from fossil fuels, where sun's energy was stored millions of years before, and from atoms, where the energy was locked from the beginning of the universe. However, an explosion in the world population, with an ever increasing demand of mankind for energy, makes the present energy supply insufficient. With the dwindling fossil fuel combined with serious health hazards and environmental pollution due to both nuclear power plant and fossil fuels, mankind is again looking towards the sun, the potential energy source, to get cheap and clean energy.

Energy flux received by the earth in one year is 3×10^{24} J. It is estimated that in one week, the planet receives the equivalent of all of its non-solar energy reserves. To tap energy from this enormous source, scientists have tried in different ways to meet the energy demand of burgeoning world population which is going to be double by 2020 as the World Energy Council (WEC) predicts. Among the various solar energy converters, photovoltaic (PV) cells are the most extensively studied and a consumer level has nearly been attained technologically. PV cells are well known for their space

CHAPTER 1. General Introduction

applications, and their terrestrial application is on the way of commercialization. They are already being used in many stand-alone applications remote from grid, such as, electric power supply to TV rebroadcast/telecommunication repeater stations [1, 2], electrification of rural community [3], electric propulsion in recreational boating [4] and in many everyday use electronic goods. But use of PV for utility and grid connected systems are yet to be proved viable economically and reliable practically. According to the National Association of Regulatory Utility Commissioners (NARUC) [5], the kWh cost of electricity generation by coal-fired steam system is \$0.08, by gas/combined cycle system is \$0.08 and by PV is \$0.24. This prohibitive high cost makes use of PV for mass generation of electricity for common consumer application unrealistic.

Given the environmental impact of conventional electricity generation and an increasing demand of energy in an ever increasing world population at hand, there is an urgent need to develop low cost sources for clean and renewable energy. Many scientists all over the world have worked for years to develop low cost, high efficiency solar cells. Table 1.1 summarizes the best reported results of some relatively cheap solar cells that are potential candidates for terrestrial application. Though the reported efficiencies of Si, CuInSe₂, and CdTe based solar cells are quite high (17.2, 16.8 and 15.8 respectively), deposition techniques for Si and CuInSe₂ are expensive and CdTe is considered as an environmental hazard. Recently, Gratzel and coworkers developed a dye-sensitized nano-

Table 1.1 : Best reported efficiency of some relatively cheap solar cells

Material	Structure	Efficiency (%)	Ref.
Si	μ c-SiC/poly-Si	17.2	[6]
CuInSe ₂	ZnO/Cu(InGa)Se	16.8	[7]
	CdS/CuInSe ₂	8.1	[8]
CdTe	CdS/CdTe	15.8	[9]
CdS	CdS/Cu ₂ S	10	[10]
TiO ₂	TiO ₂ /Dye	10	[11]

CHAPTER 1. General Introduction

crystalline (DNC) TiO_2 photoelectrochemical (PEC) solar cell [11], where a thin film of titanium dioxide, a high band gap (3.2 eV) oxide semiconductor, is coated with a monolayer of a charge-transfer dye to sensitize the film for light harvesting. Monochromatic quantum yields in the visible region of up to 100% and overall light to electric energy conversion efficiencies of 10% in simulated solar light (AM 1.5) [12] and 12% in diffused day light [11] have been reported.

The physical principle of Gratzel cell differs from the conventional solid state solar cells in the sense that the functions of light absorption and charge carrier transport are separated in these devices. In the case of *n*-type materials, such as TiO_2 , current is generated when a photon absorbed by a dye molecule gives rise to electron injection into the conduction band of the semiconductor. It is amazing that a solar cell so easy to prepare and so similar to photographic process can approach the efficiency of conventional solar cells (10~15%). One of the major advantages of the Gratzel cell is that it uses a material (TiO_2) which is cheap, abundant in nature and environmentally benign. Motivated by the exciting results of this cell, a great number of research laboratories have engaged in the development of TiO_2 based solar cells since then, which is also the main focus of this dissertation.

1.2 TiO_2 – A material of choice

It was Fujishima and Honda [13, 14] who first recognized the photocatalytic property of TiO_2 in 1971 with the observation that water could be split into oxygen and hydrogen on a biased TiO_2 single-crystal electrode upon illumination with UV light. This discovery combined with the public awareness of the need for cheap and clean energy prompted extensive research on semiconductor-liquid-junction solar cells (SLJC) using the material TiO_2 [15 - 20]. Beside SLJC, the material TiO_2 soon found its application in many other areas, to name a few, photoelectro-chemical conversion of solar to chemical energy [21-23], photocatalytic degradation of air/water pollutants [24 - 26], and photochemical methods for organic functional groups transformations and metal recovery [27-29]. It has also numerous industrial applications, such as, as a dielectric material in electronic circuits, optical coatings, as an additive in toothpaste, as a white pigment, etc.. The high popularity of

CHAPTER 1. General Introduction

this material is mainly due to its exceptional stability and ease of preparation. It can be prepared from low to medium purity materials through low-cost processes. It is also non-toxic, environmental friendly and harmless. However, as far as SLJC is concerned where a high yield is also necessary along with the stability, it performed poorly in regard to its overall energy conversion efficiency. It was found that due to the high band gap (3 eV) of TiO_2 , only 3 % of natural sunlight can be absorbed by it and overall efficiency of SLJC remains less than 1%.

Apart from TiO_2 , many other oxide-semiconductors (SrTiO_3 , Fe_2O_3 , SnO_2 , ZnO , In_2O_3 and WO_3) as well as non-oxide semiconductors (Si, Ge, CdX , GaP, GaAs, InP) were investigated for their application in solar energy conversion using water-splitting reaction. However, it was soon realized that none of the oxide semiconductors possesses all the required properties for efficient photo-electrolysis, namely (i) an optimum band gap of 1.5 to 2 eV, (ii) a conduction band edge more negative than the water reduction potential combined with a valence band edge more positive than the water oxidation potential, (iii) rapid charge transfer kinetics to the electrolyte, and (iv) extreme resistance to corrosion of the semiconductor surface [30]. Further, all the non-oxide semiconductors proved to be highly corrosive in an electrolytic media.

Therefore, despite its high band gap, TiO_2 remained as a material of choice for solar energy conversion mainly due to its favorable physical and chemical properties for efficient photocatalytic reactions combined with its exceptional stability in almost all adverse electrolytic media. Huge efforts were put in the past by different groups to make TiO_2 an efficient solar cell material either by reducing the band gap by incorporating foreign elements into its lattice [31, 32] or by sensitizing TiO_2 by a low band gap material to exploit the visible region of the solar energy [33, 34]. In either case, limited success was obtained due to various factors. In 1991, Gratzel and co-workers made a breakthrough in preparing a PEC cell with an efficiency (10%) which is comparable to the conventional solid state solar cells. The introduction of this new type of cell, which is based on nano-crystalline TiO_2 deposited on a conducting glass substrate and coated with a mono-layer of dye, regalvanized the interest in TiO_2 with new hope and new prospect.

1.3 TiO₂ – Crystalline phases and structure

TiO₂ exist in three different crystalline polymorphs : rutile, anatase and brookite. Only anatase and rutile have relevance in various optical and opto-electrical applications with anatase having superior opto-electrical properties than those of rutile. Anatase form of TiO₂ is believed to be more photoactive and is characterized by wider band gap (3.2 vs. 3.0 eV), lower effective electron mass, higher mobility, shallower donor level, higher luminescence and lower dielectric constant (48 vs. 173), compared to those of rutile.

Both forms possess a rock-salt type tetragonal lattice which contains somewhat distorted octahedra. The two crystal structures differ by the distortion of each octahedron and by the assembly pattern of the octahedron chains. Fig. 1.1 shows the unit cell structures of the anatase and rutile crystals. Each Ti⁴⁺ ion is surrounded by an octahedron of six O²⁻ ions. The octahedron in rutile has a

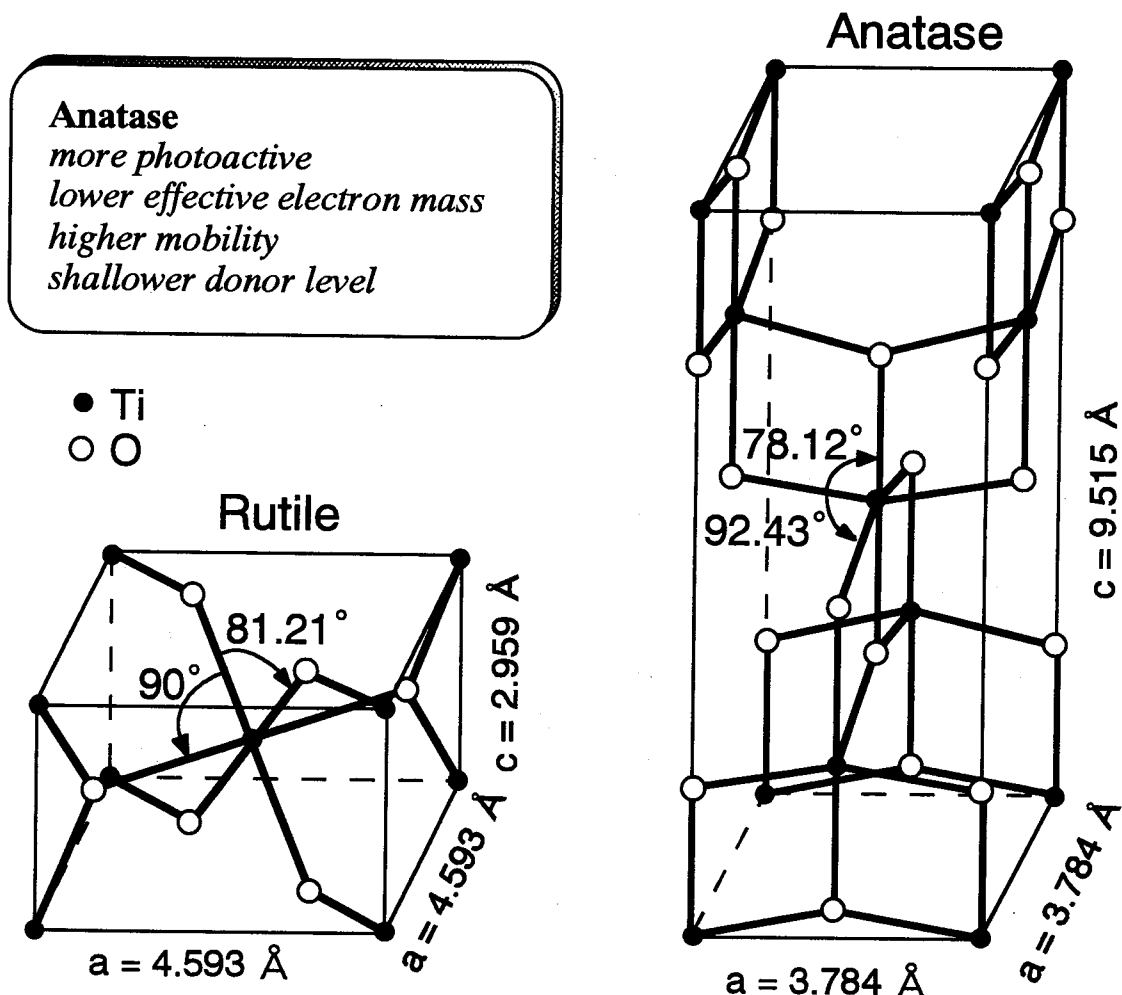


Fig. 1.1 Crystal structure of rutile and anatase TiO₂.

CHAPTER 1. General Introduction

slight orthorombic distortion while that in anatase has a significant distortion with its symmetry lower than orthorombic. Further, in anatase, each octahedron shares four edges with neighboring octahedra, whereas in rutile each octahedron shares opposite edges with neighboring octahedra, leading to formation of octahedra chains. The Ti—Ti bond distances in anatase are greater (3.79 and 3.04 Å vs. 3.57 and 2.96 Å) whereas Ti—O distances are slightly shorter than those in rutile (1.95 and 1.91 Å vs. 2.01 and 1.9 Å). Though the bond distances are not much different, greater distortion in bond angles results in a somewhat more open structure (higher molar volume, lower density) for anatase than that for rutile [35].

Both lattices are highly symmetrical with respect to titanium atoms, but not about the 3-coordinate oxygen atoms in OTi_3 units. Further, there are differing geometries of the Ti—O(Ti)—Ti units in anatase and rutile which lead to different degree of assymmetry about the oxygen atoms. This difference in the geometrical structure of OTi_3 units is supposed to be the main cause for different physical and chemical properties between anatase and rutile [36]. Some of the basic structural and optical features of rutile and anatase modifications of TiO_2 are summarized in Table 1.2.

Small cations and anions can migrate relatively rapidly through channels in the two lattices, a process that affects the uniformity of doping and the density of recombination centers. The

Table 1.2: Some basic structural and optical features of rutile and anatase TiO_2

	Rutile	Anatase
<i>Unit cell structure</i>	Tetragonal	Tetragonal
No. of molecules per unit cell	2	4
<i>Ti—Ti distance</i>	3.57 and 2.96 Å	3.79 and 3.04 Å
<i>Ti—O distance</i>	2.01 and 1.92 Å	1.95 and 1.91 Å
<i>TiO_6 octahedra</i>	slight orthorombic distortion	symmetry lower than orthorombic
<i>OTi_3 units</i>	assymmetric	highly assymmetric
<i>Density</i>	4.25 g/cm ³	3.894 g/cm ³
<i>Band gap, E_g</i>	3.0 eV	3.2 eV
<i>Dielectric constant</i>	173	48

channel in rutile lies parallel to the c axis (perpendicular to the 001 face). It has roughly circular dimensions with an approximate radius of 0.8 Å, based on ionic radii of 0.6 Å and 1.3 Å for Ti and O, respectively [37]. In contrast, the channels in anatase run perpendicularly to the c axis and to each other.

Rutile is thermodynamically more stable than anatase at room temperature; the free energy change for anatase to rutile is -5.4 KJ/mol [38]. Anatase can be converted to rutile at high temperatures. The rate of conversion does not become significant until temperatures above 500 °C, and depends on the sample morphology, the nature of any impurities present [39], and the ambient atmosphere [40] as well as the temperature.

Theoretical calculations of the energy band structure of rutile have been reported by Goodenough [41], Vos [42], Daude *et al.* [43], and Munnix and Schmeits [44]. The upper edge of the valence band arises from O (2p) atomic orbitals which form π -bonding orbitals. The lower part of the conduction band originates predominantly from Ti (3d) atomic orbitals and contains a t_{2g} -like nonbonding band and an e_g -like π^* band. The detailed calculations of the band structure of anatase are yet to be carried out.

1.4 DNC solar cell – Problems and prospect

Considering the positive aspects of TiO_2 on one hand and the high demand for cheap and renewable energy on the other, a great deal of research effort has been put in the past several years to reproduce and improve the Gratzel cell. However, though few groups [45] claim to have achieved high efficiency (9.2%) close to that reported by Gratzel (10%), there is a widespread controversy about the reproducibility of the Gratzel cell and efficiency obtained by most of the groups is only 6 ~ 7 % [46, 47]. Gratzel cell is also currently being faced with a number of practical challenges. The cell, though efficient in charge transfer and free from electron-hole recombination loss, suffers a lack of stability and the dye sensitizer is prone to chemical degradation. Further, the liquid electrolyte is easy to get evaporated when the cell is imperfectly sealed, and more generally diffusion and reaction of

CHAPTER 1. General Introduction

water or oxygen molecules may worsen the cell performance. Also, due to the presence of liquid electrolyte manufacture of multi-cell module is difficult because the cells must be connected electrically yet separated chemically, preferably on a single substrate. These difficulties have made the production of the cell on a commercial basis improbable despite its low cost ($0.07 \sim 0.10 \text{ \$/kWh}$) [47] and simple fabrication technique.

Considering these aspects, several groups concentrated their efforts for the development of a solid-state prototype of the DNC solar cell. One idea was to substitute the liquid electrolyte with a *p*-type semiconductor to scavenge the hole from the photo-excited dye. Tennakone *et al.* [48] reported the first such solid-state dye-sensitized heterojunction solar cell of structure $\text{TiO}_2/\text{dye}/\text{CuI}$, where CuI is a high band gap ($>2.8 \text{ eV}$) *p*-type transparent semiconductor. A short-circuit current of 2.5 mA/cm^2 , open-circuit voltage of about 375 mV , and an over all efficiency of about 0.8% were obtained with such a cell. Regan *et al.* [49] reported similar solid-state prototype, $\text{TiO}_2/\text{dye}/\text{p-CuSCN}$, where they made use of *p*-CuSCN to substitute the electrolyte. Though a reasonable good open-circuit voltage ($\sim 500 \text{ mV}$) was obtained, photocurrent was only in the micro-ampere range. Cao *et al.* [50] reported a quasi-solid-state cell where they used ionic conducting polymer, prepared by gelation using polyacrylonitrile, instead of the liquid electrolyte. However, low quantum yield was observed and was explained as due to incomplete wetting of the nano-structured porous TiO_2 film by the polymer electrolyte. More recently, Bach *et al.* [51] introduced an amorphous conducting material, which is actually an organic hole transport material (HTM) where positive charge hope from one molecule to another, to replace the liquid electrolyte. One major advantage of this material is that since the material is in amorphous state, it would make better contact at the interface with the dye-coated TiO_2 than would a crystalline state, ensuring efficient hole transport from the oxydized dye to the HTM. Though the cell performance is poor and the efficiency is low (0.70%), the new material does show the prospect for cheap, large area solid-state dye sensitized solar cell.

Another idea towards solid-state prototype of DNC cell is to replace the dye with a polymer

CHAPTER 1. General Introduction

or a *p*-type semiconductor which will result in an all solid-state nano-crystalline TiO₂ solar cell. Kajihara *et al.* [52] reported a photovoltaic cell of structure ITO/TiO₂/polythiophene (PT)/Au. The superiority of PT over organic dye is that it is mechanically tough and its electrical properties are negligibly affected by air. However, the efficiency obtained with this structure was quite low (0.008%) and is attributed to the poor contact between the nano-crystallites and PT, specially in the interior of the film. In order to obtain intimate contact between the nano-crystals and the polymer, a conjugate polymer-semiconductor nanocrystal device (Al/polymer-nanocrystal composite/SnO₂:F-glass) was fabricated by Salafsky *et al.* [53]. Again, only limited success has been obtained with this structure. An all solid-state *p-n* heterojunction solar cell of structure SnO₂/TiO₂/a-Si:Hi/Pt with an efficiency of around 1% has been reported by Konenkanp *et al.* [54]. Poor contact at the interface and coverage of only a small fraction of the total internal surface area of the film by a-Si led to low yield of such a cell. Deposition of quantum dots of PbS on nano-crystalline TiO₂ was perceived as a possible way of obtaining intimate contact to the internal surface of TiO₂. However much remains to develop the system before any reasonably good efficiency can be achieved from this structure.

The main problem in all sorts of solid-state TiO₂ solar cell structures addressed so far lies in having a good contact with the nano-crystallites of TiO₂. Therefore, for solid-state solar cell application, one may consider the use of a TiO₂ film with a flat surface which will result in a better contact though at the expense of a huge decrease in effective surface area. However, a semiconductor with high absorption coefficient must be chosen as the main absorber material in this case to get an efficient *n-p* heterojunction solar cell structure. The high effective surface area of TiO₂ film, which is necessary for a DNC cell to ensure maximum possible solar energy absorption, will not be required any more once the absorber layer has a high absorption coefficient and enough thickness. Such a cell structure, namely, *n*-TiO₂/*p*-CuInSe₂, is proposed and its modification for better performance is described in chapter 4 of this dissertation. CuInSe₂ is chosen as an absorber material because of its low band gap and extremely high absorption coefficient.

1.5 Purpose and organization of this dissertation

With the depleting energy resources and increased environmental pollution due to fossil fuel, the ever increasing demand for cheap and clean energy can be met by the development of efficient and cost-effective solar cells. The purpose of this dissertation is aimed at developing low cost solar cells based on an environmentally benign oxide semiconductor such as TiO_2 , which is cheap, easy to prepare, non-toxic and abundant in nature.

In contrast to the rutile modification of TiO_2 which is well studied, the anatase modification, which has gained the central focus only recently after the Gratzel cell and is considered as a potential material for photovoltaics, is still under investigation for its various optical and electrical properties. Therefore, before experimenting with solar cell, we have explored various structural, optical and electrical properties of nano-crystalline TiO_2 thin films deposited by a sol-gel method which are described in the following chapter (chapter 2). Among various existing methods, we have employed sol-gel dip-coating method to prepare the nano-crystalline films and the effect of annealing temperature on crystal structure, crystallinity and growth of various phases, and other film properties are studied in detail.

Dye-sensitized solar cell based on nano-crystalline TiO_2 has attracted much attention due to its low cost and simple fabrication technique. However, much remains to understand fully the device mechanism and various problems associated with its fabrication in order to reproduce the 10% efficient Gratzel's cell. In chapter 3, we will give a brief introduction of this new type of cell, its preparation and operating principles, and will report the results of our preliminary investigation on DNC cells with the TiO_2 films being prepared by spreading the colloidal TiO_2 paste using a glass rod and by sol-gel dip-coating method. Slight addition of triton-X to the TiO_2 paste, which is usually added to assist the spreading of the sol on the substrate, has been found to have a profound effect on cell performance. Details of the effect of triton-X addition on the surface morphology of TiO_2 film and cell performance will be described in this chapter. In the sol-gel dip-coating method, effect of pulling speed on cell performance is studied.

CHAPTER 1. General Introduction

As has already been described in section 1.4, the DNC cell, developed by Gratzel and his group, though very attractive due to its low cost and simple fabrication technique, suffers a lack of stability due to organo-metallic dye and liquid electrolyte. Therefore, it is worthwhile to look into the possibility of developing a solid-state solar cell using the low cost thin film of TiO_2 as the window material and any other suitable semiconductor as the base material. Among various semiconductors, CuInSe_2 is known to be a good material for photovoltaic devices. It has a low band gap (1.04 eV), high absorption coefficient and stable opto-electrical characteristics. In chapter 4, first, a model for our proposed $n\text{-TiO}_2/p\text{-CuInSe}_2$ heterojunction solar cell has been developed and its efficiency has been calculated in order to find out its feasibility as a photovoltaic energy converter. Our model is developed using the established theories of current conduction mechanism in Schottky barrier diodes with a varying barrier height as the junction voltage of the cell varies.

Despite the potential prospect of TiO_2 in making low cost heterojunction solar cell in conjunction with CuInSe_2 , a close look at the band diagram of $\text{TiO}_2/\text{CuInSe}_2$ heterojunction reveals the fact that TiO_2 is not a good match for CuInSe_2 . Because of the mismatch between electron affinities of TiO_2 (4 eV) and CuInSe_2 (4.48 eV), there exists a high spike at the conduction band edges of $\text{TiO}_2/\text{CuInSe}_2$ heterojunction which will hinder the flow of photo-generated electrons from CuInSe_2 to TiO_2 and will keep the cell efficiency to a low value. A theoretical efficiency of about 1.51% has been calculated under ideal conditions, i.e., neglecting recombination losses and the effects of series and shunt resistances.

Therefore, to reduce this high barrier, a new solar cell material $\text{Pb}_x\text{Ti}_{1-x}\text{O}_2$ is proposed as a window material of the cell instead of TiO_2 , and a theoretical study of the performance of such a cell is also made and is discussed in chapter 4. Theoretical work of Krishna *et al.*[55] reveals the possibility of reducing the band gap of TiO_2 by doping it with Pb, hence the material $\text{Pb}_x\text{Ti}_{1-x}\text{O}_2$. In our calculation, it is assumed that the electron affinities of the two semiconductors are perfectly matched and that the band gap of $\text{Pb}_x\text{Ti}_{1-x}\text{O}_2$ is 2.58 eV. The assumption of these values closely matches with the theoretical calculations when PbO_2 and TiO_2 are mixed at a ratio of 1:3 [55]. An efficiency of as

CHAPTER 1. General Introduction

high as 18.78% has been calculated theoretically for this cell with the configuration $n\text{-Pb}_x\text{Ti}_{1-x}\text{O}_2/p\text{-CuInSe}_2$, assuming perfect matching of the conduction band edges.

In chapter 5, we have reported the results of our preliminary attempt to produce $\text{Pb}_x\text{Ti}_{1-x}\text{O}_2$ material in thin film form by a simple sol-gel method in order to obtain a reduction in the band gap and an increase in the electron affinity of TiO_2 . A gradual decrease in the band gap has been observed as the content of Pb is increased into the TiO_2 lattice. Various structural, optical, compositional and chemical analyses of the films are carried out using standard analytical techniques and are discussed in detail in this chapter.

Finally, in chapter 6, a summary and few remarks on the future scope of this work are given.

References

- [1] H.F. Ramos, *Tech. Dig. on IEEE First World Conference on Photovoltaic Energy Conversion*, Hawaii, 1994, p. 1141.
- [2] J.A. Gregory, A.S. Bahaj and R.S. Stainton, *Tech. Dig. on IEEE First World Conference on Photovoltaic Energy Conversion*, Hawaii, 1994, p. 1149.
- [3] J.M. Huacuz, J. Agredano, G. Munguia, R. Flores, *Tech. Dig. on IEEE First World Conference on Photovoltaic Energy Conversion*, Hawaii, 1994, p. 1134.
- [4] G. Loois, F. P. H. Wouters, G. M. Koertsand, T. C. J. V. Weiden, *Tech. Dig. on IEEE First World Conference on Photovoltaic Energy Conversion*, Hawaii, 1994, p. 1157.
- [5] National Association of Regulatory Utility Commissioners (NARUC), *Electric Power Technology : Options for Utility Generation and Storage*, NARUC Finance and Technology Committee, USA (February 1991).
- [6] W. Ma, T. Horiuchi, M. Yoshimi, K. Hattori, H. Okamoto and Y. Hamakawa, *Proc. PVSEC-6*, New Delhi, 1992, p. 463.
- [7] M. A. Contreras, J. Tuttle, A. Gabor, A. Tennant, K. Ramanathan, S. Asher, A. Franz, J. Keane, L. Wang, J. Scofield and R. Noufi, *Tech. Dig. on IEEE First World Conference on Photovoltaic Energy Conversion*, Hawaii, 1994, p. 68.
- [8] T. Nakada, N. Okano, Y. Tanaka, H. Fukuda and A. Kunioka, *Tech. Dig. on IEEE First World Conference on Photovoltaic Energy Conversion*, Hawaii, 1994, p. 95.
- [9] C. Ferekides and J. Britt, *Tech. Dig., 7th Int. PVSEC*, Japan, 1993, p. 509.
- [10] H. J. Hovel, *Semiconductors and Semimetals*, Vol. 11, R.K. Willardson and A.C. Beer (eds), Academic Press, New York, 1975, p. 195.
- [11] B. O'Regan and M. Gratzel, *Nature* **353** (1991) 737.
- [12] M.K. Nazeeruddin, A. Kay, I. Rodicio, R. Humphry-Baker, E. Muller, P. Liska, N. Vlachopoulos and M. Gratzel, *J. Am. Chem. Soc.* **115** (1993) 6382, and references therein.

CHAPTER 1. General Introduction

- [13] A. Fujishima and K. Honda, *Bull. Chem. Soc. Japan* **44** (1971) 1148.
- [14] A. Fujishima and K. Honda, *Nature* **238** (1972) 37.
- [15] G. P. A. Peter and A. F. Sammells, *Faraday Discuss. Royal Soc.* **70**, (1980) 207.
- [16] R. Memming, *Electrochem. Acta* **25**, (1980) 77.
- [17] A. J. Bard, *Ber. Bunsenges. Phys. Chem.* **92** (1988) 1187.
- [18] G. V. Subbarao, *Bull. Mater. Sci.* **10** (1988) 283.
- [19] L. M. Peter, *Chem. Rev.* **90** (1990) 753.
- [20] H. Gerischer, *J. Electroanal. Chem.* **82** (1977) 133.
- [21] P. V. Kamat and N. M. Dimitrijevic, *Solar Energy* **44** (1990) 83-98.
- [22] N. Serpone, in J. R. Norris and D. Meisel (eds), *Photochemical Energy conversion*, Elsevier Science Publishers B. V., Amsterdam, The Netherlands, 1989, p. 279-315.
- [23] M. Gratzel, in E. pelizzetti and N. Serpone (eds), *Homogeneous and Heterogeneous Photocatalysis*, D. Reidel Publishing Company, Dordrecht, The Netherlands, 1986, pp. 91-100.
- [24] O. Legrini, E. Oliveros, and A. M. Braun, *Chem. Rev.* **93** (1993) 671.
- [25] A. Mills, R. H. Davies, and D. Worsley, *Chem. Soc. Rev.* **22** (1993) 417.
- [26] M. R. Hoffmann, S. T. Martin, W. Choi, and D. W. Bahnemann, *Chem. Rev.* **95** (1995) 69.
- [27] M. A. Fox, in N. Serpone and E. pelizzetti (eds), *Photocatalysis --- Fundamentals and Applications*, John Wiley & Sons, New York, 1989, pp. 420 - 455.
- [28] M. A. Fox, *Top. Curr. Chem.* **142** (1991) p71.
- [29] M. A. Fox and M. T. Dulay, *Chem. Rev.* **93** (1993) 341.
- [30] H. O. Finklea, in *Semiconductor Electrodes*, H. O. Finklea (ed), Elsevier Science Publishers B. V., Amsterdam, The Netherlands, 1988, p. 2.
- [31] H. O. Finklea, in *Semiconductor Electrodes*, H. O. Finklea (ed), Elsevier Science Publishers B. V., Amsterdam, The Netherlands, 1988, pp. 58 - 60.

CHAPTER 1. General Introduction

- [32] Kalaga M. Krishna, Ph.D. thesis : "Theoretical and experimental determination of the band gap for some non-corrosive transition metal oxides for their use in photoelectrochemical solar cells", Indian Institute of Technology, Bombay, India, 1995.
- [33] M. T. Spitzer and M. Calvin, *J. Chem. Phys.* **66** (1977) 4294.
- [34] M. Gratzel (ed.), *Energy Resources through Photochemistry and Catalysis*, Academic Press, New York, 1983.
- [35] A. L. Linsebigler, G. Lu, and Jr. J. T. Yates, *Chem. Rev.* **95** (1995) 735 - 758.
- [36] N. Serpone and R. F. Khairutdinov, in *Semiconductor Nanoclusters - Physical, Chemical and Catalytic Aspects*, P. V. Kamat and D. Meisel (ed), Elsevier Science Publishers B. V., Amsterdam, The Netherlands, 1997, p. 419.
- [37] H. O. Finklea, in *Semiconductor Electrodes*, H. O. Finklea (ed), Elsevier Science Publishers B. V., Amsterdam, The Netherlands, 1988, p. 47.
- [38] G. V. Samsonov (ed), *The Oxide Handbook*, IFI/Plenum, NY, 1982, p. 23.
- [39] G. D. Parfitt, *Progr. in Surf. Membrane Sci.* **11** (1976) 181.
- [40] R. D. Shannon, *J. Appl. Phys.* **35** (1964) 3414.
- [41] J. B. Goodenough, *Prog. in Solid State Chem.* **5** (1971) 145.
- [42] K. Vos, *J. Phys. C* **10** (1977) 3917.
- [43] N. Daude, C. Gout and C. Jouanim, *Phys. Rev. B* **15** (1977) 3229.
- [44] S. Munnix and M. Schmeits, *Phys. Rev. B* **28** (1983) 7342.
- [45] S. K. Dev, National Renewable Energy Laboratory (NREL), Goldon, Colorado, USA; I. Lauermann, Institut fur Angewandte Photovoltaik (INAP), Gelsenkirchen, Germany.
- [46] A. Hagfeldt, B. Didriksson, T. Palmqvist, H. Lindstrom, S. Sodergren, H. Rensmo, and Lindquist, *Sol. Energy Mater. Sol. Cells* **31**, 481 (1994).
- [47] G. Smestad, C. Bignozzi and R. Argazzi, *Sol. Energy Mater. Sol. Cells* **32** (1994) 259.
- [48] K. Tennakone, G. R. R. A. Kumara, A. R. Kumarasinghe, R. G. U. Wijayantha and P. M. Sirimanne, *Semicond. Sci. Technol.* **10** (1995) 1689.

CHAPTER 1. General Introduction

- [49] B. O'Regan and D. T. Schwartz, *J. Appl. Phys.* **80** (1996) 4794.
- [50] F. Cao, G. Oskam, G. J. Meyer, and P. C. Searson, *J. Phys. Chem.* **100** (1996) 17021.
- [51] U. Bach, D. Lupo, P. Comte, J. E. Moser, F. Weissertel, J. Salbeck, H. Spreitzer, and M. Gratzel, *Nature* **395** (1998) 583.
- [52] K. Kajihira, K. Tanaka, K. Hirao, and N. Soga, *Jpn. J. Appl. Phys.* **36** (1997) 5537.
- [53] J. S. Salafsky and R. E. I. Schropp, Proceedings, *2nd World Conference on Photovoltaic Solar Energy Conversion*, 6-10 July, 1998, Vienna, Austria.
- [54] R. Konenkanp, P. Hoyer and A. Wachi, *J. Appl. Phys.* **79** (1996) 7029.
- [55] K.M. Krishna, M. Sharon, M.K. Mishra and V.R. Marathe, *Chem. Phys.* **163** (1992) 401.

Chapter 2

TiO₂ thin films by sol-gel dip-coating: structural and optical properties

2.1 Introduction

Titanium dioxide (TiO₂), perhaps the most widely studied large band gap semiconductor, has diverse industrial applications [1-5] because of its favorable physical, optical and electronic properties. Since the first demonstration of TiO₂ as a semiconductor photoanode by Fujishima and Honda in 1972 [6], extensive research has been carried out to use this material as a photoelectrode in photoelectrochemical (PEC) solar cells. The key factors which contributed to the popularity of this material are its exceptional stability in electrolytic media and ease of preparation [7]. However, its wide band gap (3 eV) set a low ceiling to the maximum possible solar to electrical power conversion efficiency of this material [8]. In 1991, Gratzel and co-workers reported a breakthrough in the development high efficiency (10-12%) dye-sensitized PEC solar cell by making use of nano-crystalline porous thin film of TiO₂ [9]. With this discovery, again, much attention has been diverted towards this classical material.

Different methods for the preparation of nano-crystalline TiO₂ thin film preparation, such as, sol-gel [10], spray pyrolysis [11], chemical vapor deposition (CVD) [12], pulsed laser irradiation [13], are reported in the literature. However, the most popular and matured techniques for semi-conductor nano-particles preparation are those based on solution synthesis route and colloidal chemical approaches rather than those on sophisticated and expensive gas phase techniques [14], though in

some cases higher growth rate with better surface morphology and homogeneity is claimed for the latter methods [15]. We have prepared nano-crystalline TiO₂ thin films by sol-gel dip-coating method, the advantage of which lies in its simplicity and low-cost. In this process, a metal-alkoxide, M(OR)_m, where M is a metal and R is an alkyl group, is hydrolyzed and polymerized by addition of water and heating the solution at a constant temperature for some hours. To get a thin film, the solution obtained, which is called as sol solution, can be spreaded over a suitable substrate by a variety of methods that includes dip-coating, spin coating or spraying. The films thus deposited are first dried at a lower temperature (< 300 °C) to remove the water and organic solvents and then annealed at a relatively higher temperature (> 400 °C) for densification and crystallization [16]. This results in a thin film of nano-crystalline oxide semiconductor particles with sponge-like structure and a porosity of as high as 50 %. Depending upon the annealing temperature and also the substrate topography, films can be amorphous or crystalline (anatase or rutile).

Rutile modification of TiO₂ is the most stable phase and its structural, optical and opto-electrical properties are well studied [17-19]. However, after the Gratzel PEC solar cell, anatase modification of TiO₂ came into focus because of its high photon to current conversion efficiency [9]. Therefore, in the following sections of this chapter where detailed structural, optical and electrical analyses of our sol-gel derived TiO₂ thin films are given, main emphasis is put on the anatase modification. Thin films of TiO₂ are deposited on different substrates (single crystal silicon, sapphire and fused quartz) under different annealing temperatures, and the effects of both the substrates and annealing temperature on crystal structure, crystallinity and growth of various phases are studied. A detailed optical characterization of the films are done using spectroscopic ellipsometry (SE), UV-visible transmittance and reflectance spectroscopy and photoluminescence (PL) spectroscopy. Effect of H₂ annealing on both the dark and photo-conductivity are also studied and the details are discussed in the following sections.

2.2 Experimental

2.2.1 Thin film preparation

TiO₂ thin films are prepared by sol-gel dip-coating method using titanium tetra-isopropoxide, Ti[(CH₃)₂CHO]₄, as the source materials for Ti. 25 ml of titanium tetra-isopropoxide was mixed with

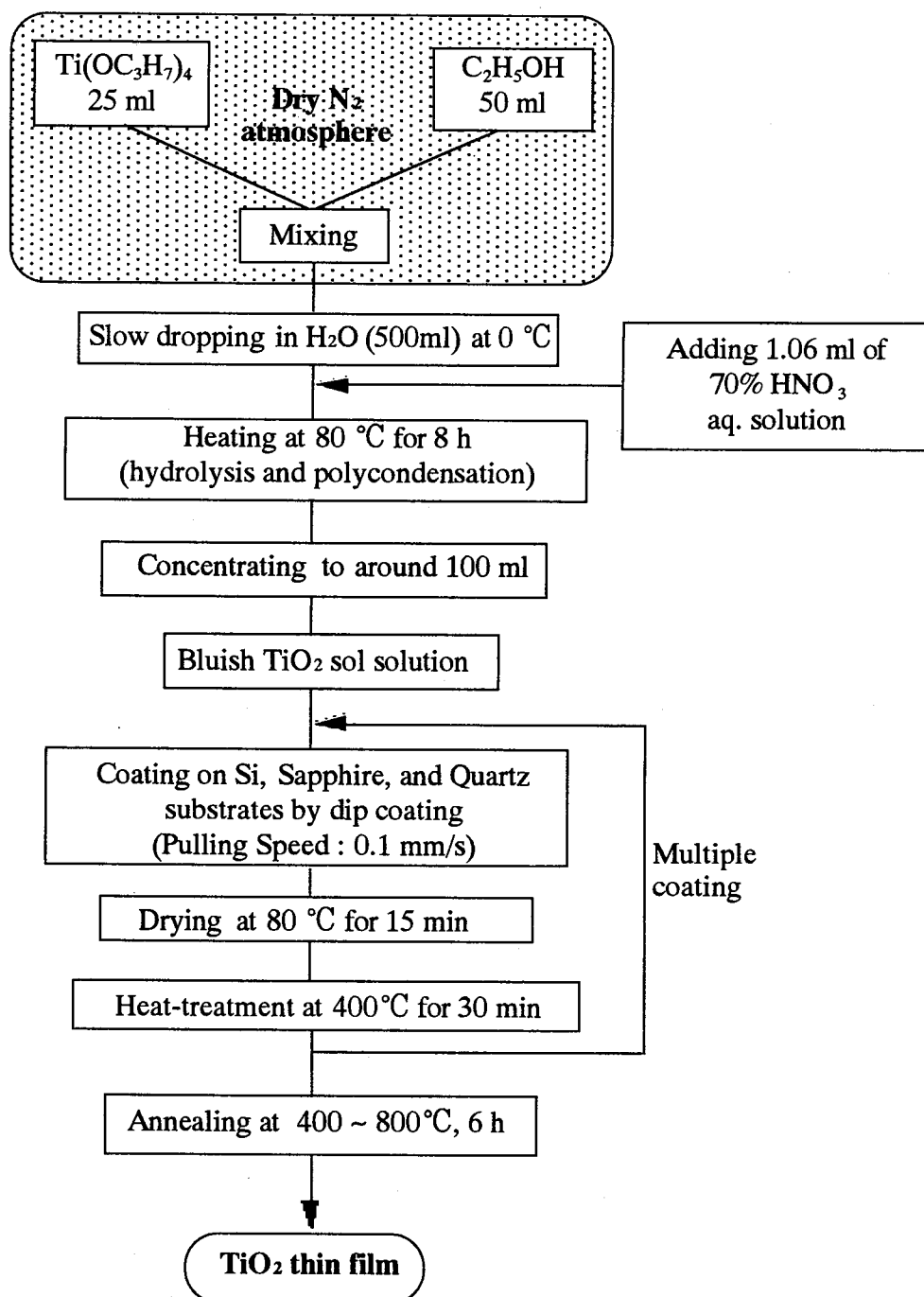


Fig. 2.1 Flow chart diagram for preparation of TiO₂ thin film by sol-gel dip-coating method

50 ml of ethanol in a dry N₂ atmosphere. The solution was then added dropwise to 500 ml of distilled water at 0 °C under stirring to carry out hydrolysis. 1.06 ml of 70 % HNO₃ aq. solution was added to this solution after which the solution was subjected to heating at 80 °C for 24 h such that the final volume will be 100 ml. Films were coated on fused quartz, single crystal Si (100), sapphire and ITO coated glass substrates by dip coating method with a pulling speed of 0.1 mm/sec. Films were dried at 80 °C for 15 min and heat-treated at 400 °C for 1 hour after each coating. The process was repeated 5 times and finally the films were annealed at 400, 600 and 800 °C, respectively, for 6 hours, at a constant heating rate of 5 °C /min. The details of the sol solution preparation and the thin film deposition are elucidated in the flow chart diagram of Fig. 2.1.

2.2.2 Characterization

Crystal structure, growth and crystallinity of various phases of these films were studied by X-ray diffraction (Rigaku Rint-1100) using CuK α radiation (1.5406 Å) as an X-ray source and at a scanning rate of 1° min⁻¹. Thickness measurement and surface morphology study of the films were done by a scanning electron microscope (Hitachi S-5000).

Optical properties of the films have been studied using spectroscopic ellipsometry, UV-visible spectroscopy and photoluminescence spectroscopy. The measurements of spectroscopic ellipsometry have been carried out at an angle of incidence of 70° in the wavelength range of 260~830 nm. The optical properties of thin films were fitted directly to measured spectroscopic ellipsometry (Δ , Ψ) data using classical dispersion formula. PL measurements were carried out at room and liquid nitrogen temperature using 325 nm He-Cd laser source.

Conductivity study has been carried out for the films deposited on both ITO coated glass and fused quartz substrates. Silver paste has been used to make ohmic contacts on both TiO₂ and ITO surface. Films are annealed in H₂ atmosphere under different temperature conditions and both dark and photo-conductivity have been investigated by using a solar simulator at 1 sun AM0 conditions.

2.3 Results and discussion

2.3.1 Structural

2.3.1.1 X-ray diffraction

XRD patterns of TiO₂ thin films, deposited on quartz, sapphire and silicon substrates, both as-deposited and annealed (800 °C, 6 h), are shown in Fig. 2.2. The films deposited on different substrates, under same conditions show different structural properties. The as - deposited films on sapphire and silicon substrates are polycrystalline, single phase, anatase (A) type, while that on quartz substrate are amorphous, may be due to the amorphous nature of the quartz substrate which inhibits crystallization process. After annealing the samples at 800 °C for 6 h, the films on quartz and sapphire substrates are transformed completely into rutile (R) phase while that on the Si substrate is highly anatase type with simultaneous presence of small rutile phase (Fig. 2.2, patterns a', b' and c'). This is explained in the following way. The crystal structure of Si, which is cubic, retards the transformation of anatase phase to rutile at higher temperature while that of sapphire, which is same as that of rutile phase of TiO₂ (tetragonal), favors the formation of rutile phase at high temperature. However quartz substrate, due to its amorphous nature, probably does not have any effect on anatase or rutile phase formation. Films are rutile on quartz at 800 °C with poor crystallinity, evidenced by the weak X-ray peak intensities (Fig. 2.2, pattern a'), may be due to the amorphous nature of the substrate.

The results from XRD patterns of all the samples, deposited on three different substrates under different deposition conditions, are summarized in Table 2.1. Table 2.1 reveals the films are polycrystalline, anatase type until 600 °C annealing temperature for all the substrates, above which (800 °C) films are rutile or a mixture of A/R, depending on substrate topography. Our observation is in agreement with that reported by Yuan *et al.* [20], where they reported that sol-gel derived TiO₂ thin films are anatase type until 600 °C annealing temperature and a mixture of A/R in the temperature range 600-900 °C.

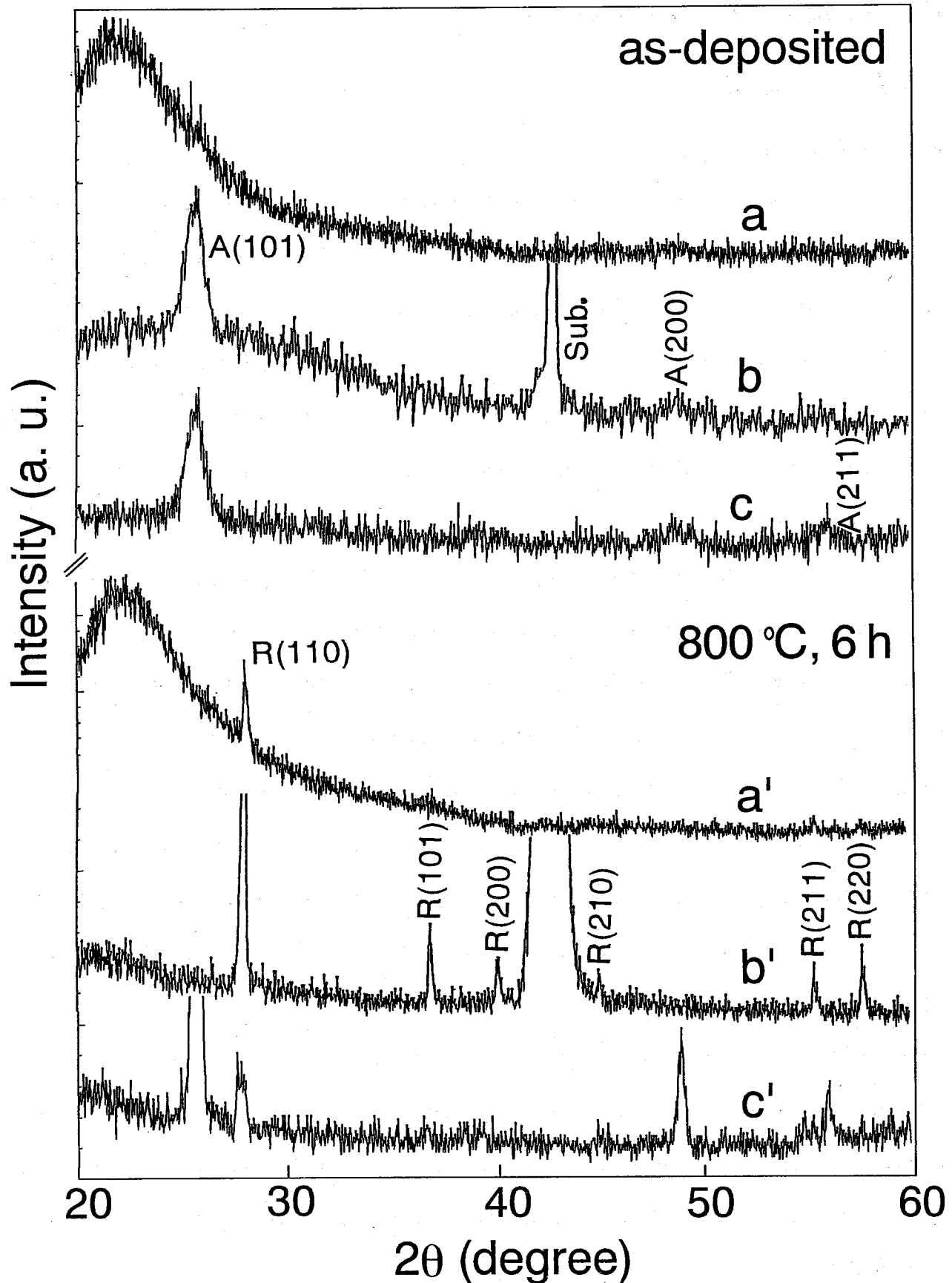


Fig. 2.2 XRD patterns of as-deposited and annealed (800°C , 6 h) TiO_2 thin films, deposited on quartz (a, a'), sapphire (b, b') and silicon (c, c') substrates, by sol-gel process.

TABLE 2.1 : Summary of XRD results

Annealing Condition \ Substrate	Quartz	Sapphire	Silicon
As-deposited	amorphous	A	A
400 °C, 6 h	A/amorphous	A	A
600 °C, 6 h	A	A	A
800 °C, 6 h	R	R	A(90.7%)/R(9.3%)

(A: Anatase; R: Rutile)

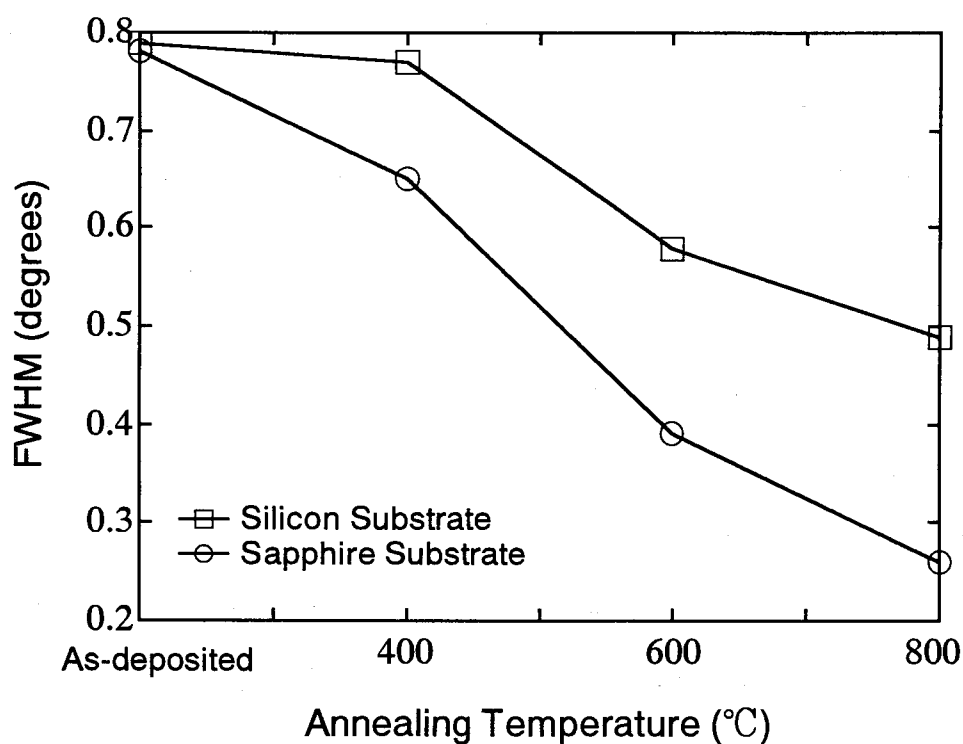


Fig. 2.3 A plot of FWHM of the 100 % X-ray peak corresponding to A(101)/R(110) plane of the as-deposited and different temperature annealed TiO_2 thinfilms, deposited on silicon and sapphire substrates, respectively.

Full width at half maximum (FWHM) of the X-ray peak intensity (Fig.2.3), corresponding to 100% A(101)/R(110) plane of TiO_2 films, has been found to decrease with increase in annealing temperature for all the substrates, with that for sapphire substrate being smallest for all deposition conditions, indicating better crystallinity of the films on sapphire substrate compared to others.

2.3.1.2 Scanning electron microscopy

Figure 2.4 shows the SEM surface morphology of TiO₂ thin films deposited on Si substrate, annealed at different temperatures. These micrographs reveal nano-crystalline nano-porous structure of the films with crystal size varying from 8-10 nm to 50-150 nm range depending upon annealing temperature. The increase in particle size with increase in annealing temperature is in consistent with XRD results where we observed decrease in FWHM with annealing temperature. While at low annealing temperature, the particles are essentially of uniform size, at high annealing temperature evolution of particles of different size and shape with clear crystal facets can be observed. This may be due to the fact that at high temperature transformation of anatase phase to rutile takes place, as observed by the XRD pattern (Fig. 2.2, pattern c') which shows the presence of rutile phase as well along with that of anatase, and results in crystallites of non-uniform size and shape.

2.3.2 Optical

2.3.2.1 Spectroscopic ellipsometry

(i) Theoretical considerations

The measurements of spectroscopic ellipsometry have been carried out for the samples deposited on Si substrates at an angle of incidence of 70° in the wavelength range of 260~830 nm. Hereafter the as-deposited and annealed (400, 600 and 800 °C) samples will be referred to as samples 1 through 4, respectively. The optical constants of thin films were calculated assuming a structure of TiO₂/Si for the low temperature annealed samples (samples 1, 2 and 3) and TiO₂/SiO₂/Si for the high temperature annealed sample (sample 4). Data used for Si were taken from literature [21]. Classical dispersion formula was used for the analysis. Surface roughness, which is usually considered for ellipsometric determination of optical constants of oxide thin films by assuming a separate thin layer on the surface [22-24], is not considered for the analyses of our films. Since our sol-gel derived TiO₂ thin films are porous and the pores are present not only on the surface but are distributed uniformly

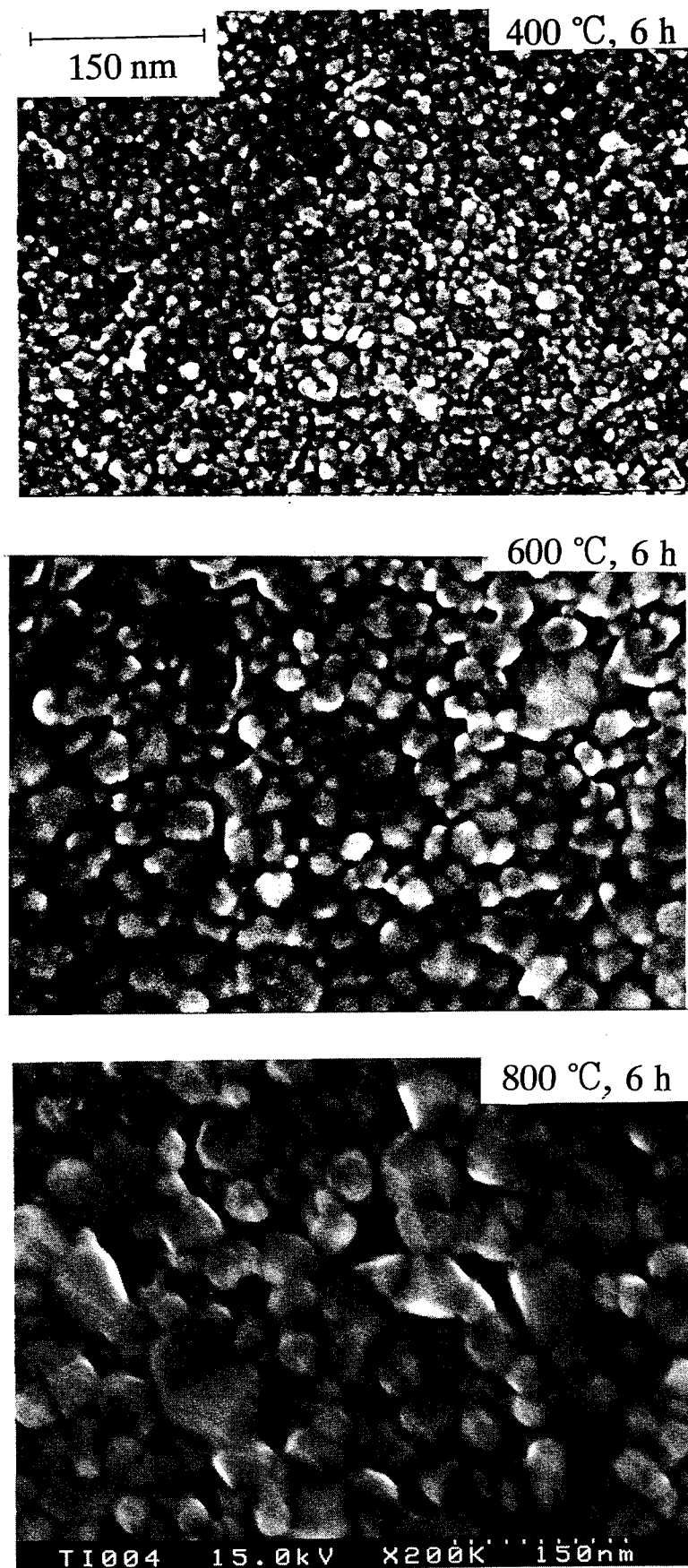


Fig. 2.4 SEM surface morphology of TiO_2 thin films deposited on Si substrate and annealed at different temperatures.

along the thickness of the films, the structure of the films can be considered to be consisting of one single layer. For discontinuous films, as is ours, the optical constants of the films are usually determined from the known bulk data and void fraction, using an effective medium theory [25]. However, there are practical difficulties associated with various effective medium models such as knowing the exact optical constants of the bulk material, knowledge of the size and shape of the grains etc., and these are well described in Ref. 26. Therefore, these models are not used for the calculation of optical constants of our films. Instead, only the pseudo (effective) optical constants of the films resulting in the best fit between the experimental and calculated data are determined. The films are also considered to be homogeneous with no grading in the density. These assumptions are justified as good fit is obtained between the experimental and calculated data, as discussed in the following sections.

(ii) Fitting analysis

The spectroscopic ellipsometry measurements are carried out for all four samples that are deposited on Si substrate and annealed at different conditions. In order to obtain the thickness and optical constants of TiO₂ films simultaneously, the optical properties of TiO₂ were fitted by using the following classical dispersion formula

$$\epsilon = \epsilon'_{\infty} + \frac{(\epsilon_s - \epsilon'_{\infty})\omega_t^2}{\omega_t^2 - \omega^2 + i\Gamma_0\omega} + \frac{\omega_p^2}{-\omega^2 + i\Gamma_D\omega}$$

where ϵ'_{∞} represents the high-frequency dielectric constant, ϵ_s the static dielectric constant, ω_t the frequency and Γ_0 the damping factor of the oscillator, ω_p the frequency correlated to the plasma term, and Γ_D the connected damping factor. Simulated and experimental data were analyzed by a Levenberg -Marquardt minimization routine [27] based on comparison of the data with the mode for the structure using the error function δ :

$$\delta^2 = \frac{1}{2N - M} \sum_i^N \left[(\tan \Psi^{cal} - \tan \Psi^{exp})^2 + (\cos \Delta^{cal} - \cos \Delta^{exp})^2 \right]$$

where N is the number of measured Ψ and Δ pairs and M is the total number of real valued fit

parameters.

For samples 1-3, one layer model (TiO_2/Si) was used to fit the calculated data with the measured data. No interfacial layer that might develop between the TiO_2 thin film and Si substrate was assumed for the fitting. However, for sample 4, which was annealed at higher temperature (800 °C), an interfacial layer of SiO_2 has been considered to obtain a satisfactory fit. Cross-sectional view by SEM micrographs for samples 1 to 3 show no detectable interfacial layer and a typical micrograph of

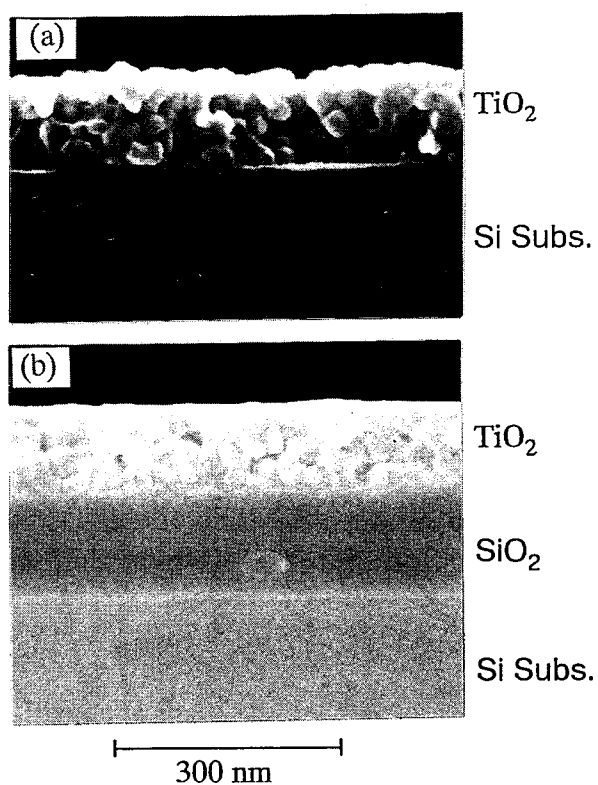


Fig. 2.5 Cross-sectional scanning electron micrographs of nano-crystalline TiO_2 thin films, deposited on Si substrate: (a) sample 3, (b) sample 4.

sample 3 is shown in Fig. 2.5a. However, coincidentally sample 4 (Fig. 2.5b) does show an interfacial layer almost as thick as the TiO_2 film and agree with our theoretical assumption of this layer used to get a good fit. The interfacial SiO_2 layer would have formed during the high temperature annealing in normal atmosphere. The fitting results of measured Δ and Ψ spectra are shown in Fig. 2.6 (a-d). The graphs show an excellent fit for all the samples, in the wavelength range 350-830 nm. The deviation of the fit from the experimental data above 3.5 eV may be due to the interband transitions.

The thickness and coefficients of different measurements and fittings are listed in Table 2.2.

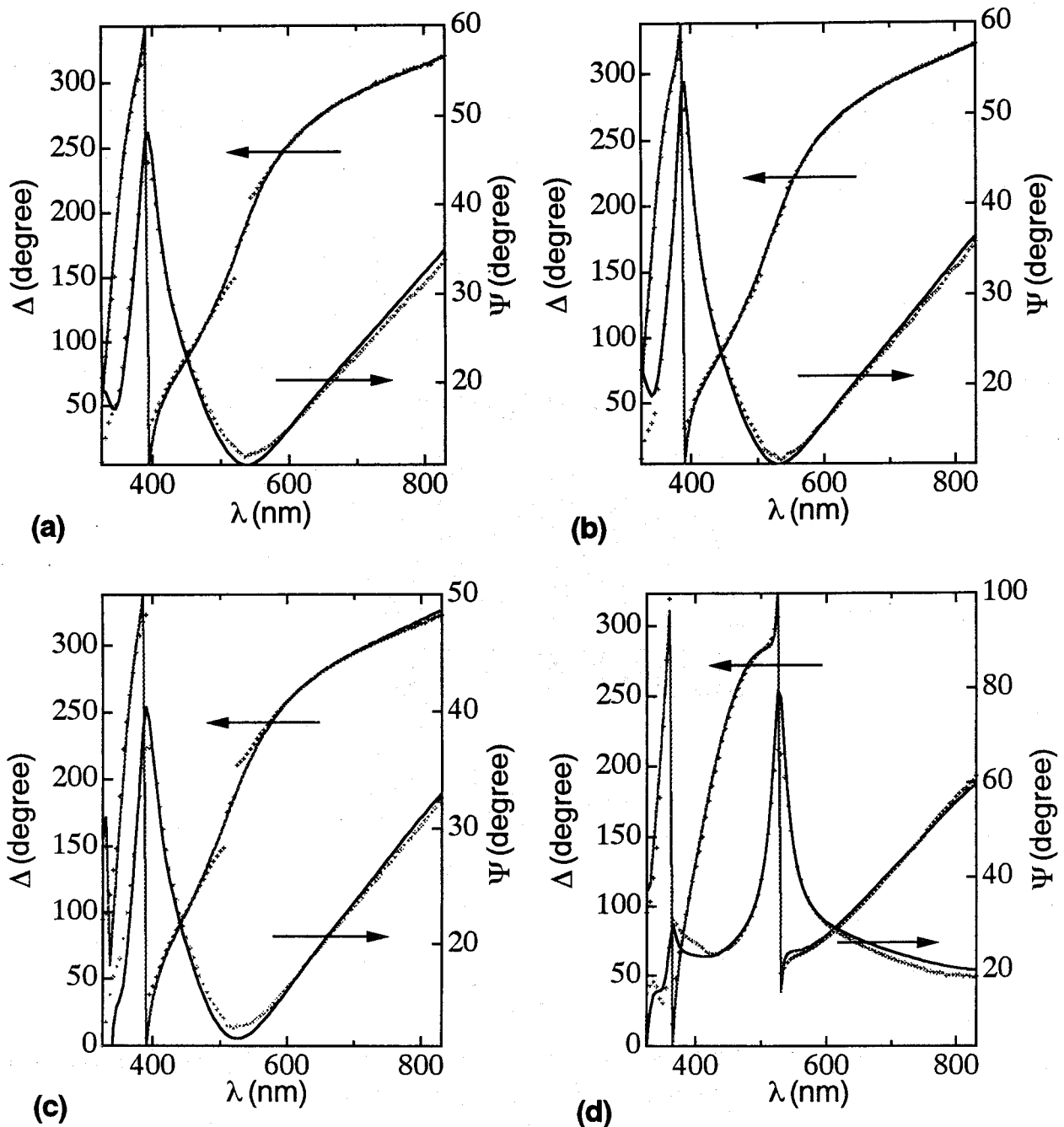


Fig. 2.6 Δ and Ψ , measured (dotted lines) and fitted (solid lines), spectra of nano-crystalline TiO_2 thin films, deposited on Si substrate: graphs (a) to (d) represent samples 1 to 4.

The thickness and coefficients of different measurements and fittings are listed in Table 2.2. Gradual decrease in the thickness with increasing annealing temperature is observed, may be due to increased packing density of the films as also evidenced by SEM cross-sectional micrographs (Fig. 2.5) which show the 800 °C temperature annealed sample to be more densely packed with less voids than the 600 °C temperature annealed sample. Furthermore, similar conclusions were also derived by

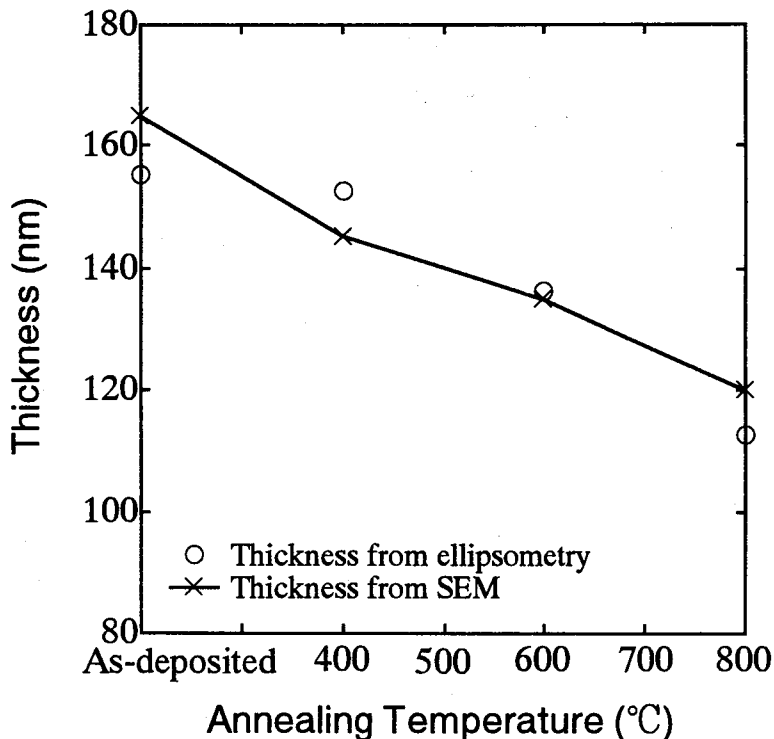


Fig. 2.7. Plot of thickness vs. annealing temperature for nano-crystalline TiO_2 thin films, deposited on Si Substrates, annealed at different temperatures.

Vorotilov *et al.* [28] for sol-gel derived TiO_2 thin films. Figure 2.7 shows the pictorial representation of gradual decrease in film thickness with increasing annealing temperature. Film thicknesses obtained for both TiO_2 and SiO_2 layers by spectroscopic ellipsometry are in good agreement with SEM cross-sectional thickness measurements.

The high-frequency dielectric constant, ε'_∞ , is in the range of 2.51-3.44 and increases with increasing annealing temperature. The values of ω_p found are between 0.41 and 0.70 eV. The plasma frequency ω_p represents the oscillation of free electrons in the conduction band of TiO_2 . To our knowledge, these are the first reported results on the value of ω_p for nano-crystalline TiO_2 thin film, and we compare our results with those obtained for indium tin oxide (ITO) films (between 0.68 and 0.96 eV) by Gerfin *et al.* [23] to explain in the following way. Values of ω_p obtained for our TiO_2 films are less than those obtained for ITO films by Gerfin *et al.*. Since ITO is a conductive oxide with high concentration of conduction electrons and TiO_2 is a semiconductor with high resistivity, smaller value of ω_p , i.e., smaller carrier concentration for TiO_2 is in accordance with what is expected.

The plasma frequency ω_p is related to the electron carrier concentration by [29],

$$\omega_p = \sqrt{\frac{ne^2}{\epsilon_0 m}}$$

where n is the electron carrier concentration, e is the electronic charge, ϵ_0 is the permittivity of free space and m is effective electron mass. We presume that our as-deposited TiO₂ films are *n*-type with carrier concentration originating from non-stoichiometry or oxygen vacancies which can be described

Table 2.2. Film thicknesses, coefficients of the classical dispersion formula and the error function for the four samples, obtained by fitting SE data measured at an incidence angle of 70°.

Sample No.	Thickness of TiO ₂ (nm)	Thickness of SiO ₂ (nm)	ϵ'_{∞}	ϵ_s	ω_t (eV)	Γ_0 (eV)	ω_p (eV)	Γ_D (eV)	δ
1	155.2	0	2.51	3.51	4.34	0.15	0.41	2.73	0.05
2	152.6	0	2.66	3.48	4.26	0.10	0.43	2.13	0.04
3	136.2	0	3.18	4.0	3.96	0.14	0.63	1.13	0.123
4	112.5	142.9	3.44	5.22	4.22	0.20	0.70	0.42	0.284

as Ti³⁺—V_o—Ti³⁺ according to Goodenough [18]. Presence of Ti³⁺ species in our sol-gel derived TiO₂ thin films is confirmed by X-ray photoelectron spectroscopy (XPS) measurement. As also can be seen from table 2.2 that damping factor Γ_D , related with the plasma oscillation, decreases gradually from sample 1 to sample 3 and for sample 4 it decreases to a very low value. We believe that since fitting analysis for sample 4 involves more parameters because of the presence of extra SiO₂ layer, the value obtained for Γ_D is much deviated from its true value and should be regarded as a mathematical entity only.

The computed refractive index (n) and extinction coefficient (k) spectra of the films together are shown in Fig. 2.8. There is a gradual increase in the refractive index as the as-deposited samples are annealed at higher temperatures (up to 600 °C) and at a much more elevated temperature (800 °C), a

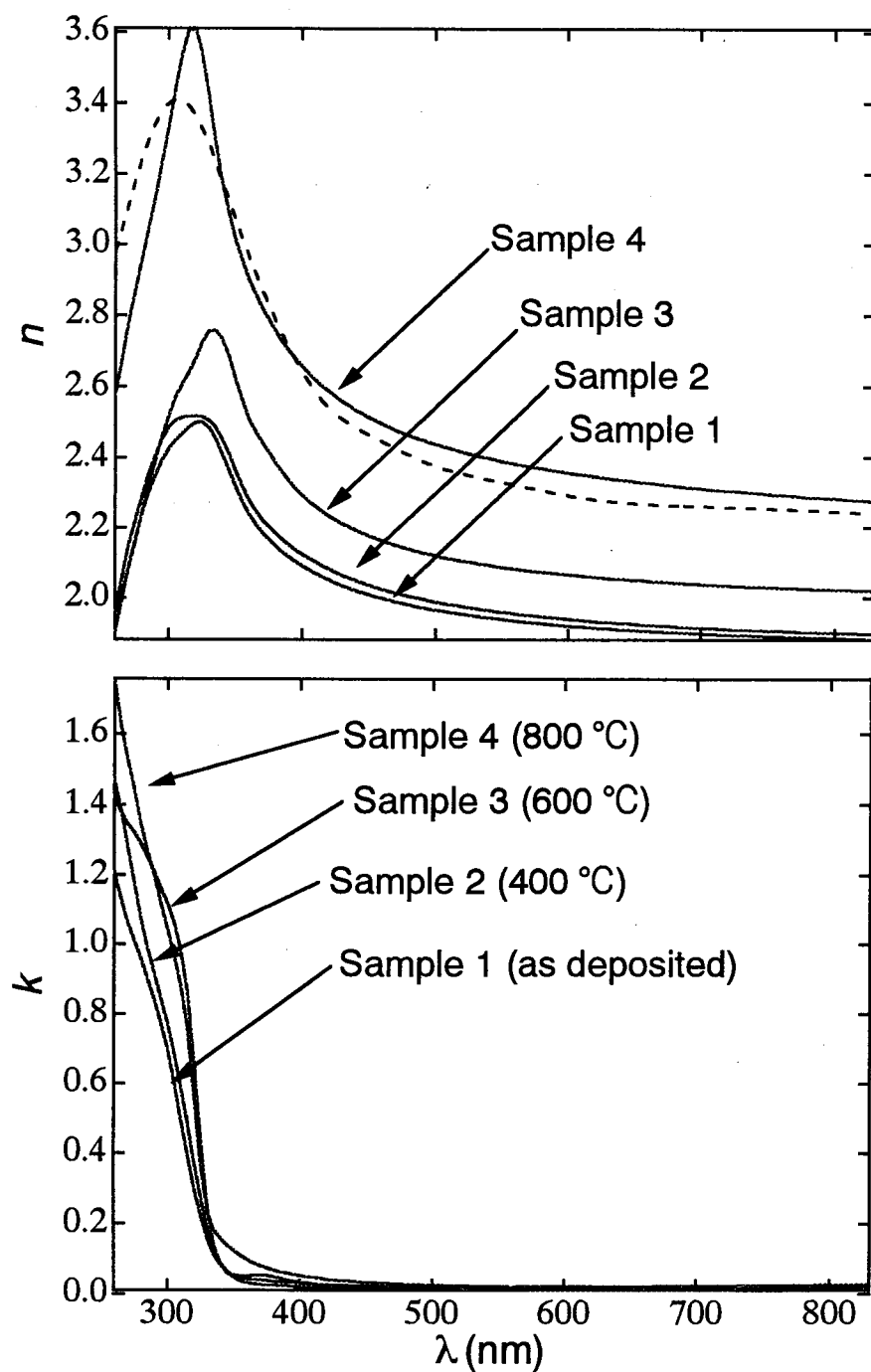


Fig. 2.8 Refractive index n (top) and extinction coefficient k (bottom) spectra of nano-crystalline TiO_2 thin films, deposited on Si substrates. The dashed line shows the refractive index spectrum of electron beam evaporated TiO_2 films on fused quartz, by Kim [25].

sharp increase in the refractive index is observed (Fig. 2.8, top). This increase in refractive index with annealing temperature is attributed to the increase in packing density and crystallinity of the films which are also evident from the XRD patterns (Fig. 2.2) and SEM micrographs (Fig. 2.5).

Furthermore, sharp increase in n above 600 °C may be due to the enhanced crystallinity of the TiO₂ films, evidenced by the intense sharp X-ray peak at this elevated temperature (XRD pattern c', Fig. 2.2) as compared to those annealed at lower temperatures. These results are in very good agreement with those by Suhail *et al.* [30], for magnetron sputtered TiO₂ thin films, where they reported similar increase in the refractive index with increasing annealing temperature and a sharp increase above 600 °C. Our as-deposited sample (sample 1) shows a refractive index of 1.97 at 500 nm which has increased to 2.44 for the sample annealed at 800 °C (sample 4). These values are in close agreement with those reported by others[26, 27, 31].

For direct comparison purpose, refractive index spectrum of electron beam evaporated TiO₂ thin films, deposited on fused quartz substrate, by Kim [22], is shown by the dashed line in Fig. 2.8 along with the refractive index spectra of our films. This spectrum closely matches with the spectrum of the high temperature annealed sample (sample 4). The as-deposited (sample 1) and low temperature annealed (samples 2 and 3) samples have a lower value of n than that for electron beam evaporated TiO₂ thin film. We believe that this is due to the low film density and high percentage of void of these films which are common characteristics for sol-gel derived films. However, there is a gradual increase in film packing density, consequently an increase in the refractive index, as the films are annealed at higher temperatures.

The extinction coefficient (k) spectra of our films (Fig. 2.8, bottom) resemble that reported by Memarzadeh *et al.*[26] for magnetron sputtered TiO₂ thin films on glass substrate. Measurement of k , where absorption is very small, is not very accurate with spectroscopic ellipsometry. However, within the accuracy limit, the k spectra do not show any significant absorption in the wavelength region lower than the band gap energy of anatase form of TiO₂ (3.2 eV). Strong absorption above the band gap energy together with the sharp peaks in the n spectra show good crystallinity of the films.

The onset of the increase in the k values at around 380 nm is due to the indirect transition followed by a mixture of direct and indirect transitions at lower wavelength, i.e., higher energy region.

2.3.2.2 UV-visible spectroscopy

Figure 2.9 shows the transmittance (top) and reflectance (bottom) spectra of both as-deposited and annealed TiO₂ thin films, deposited on quartz substrate. All the transmittance spectra show a sharp decrease in the transmittance at around 390-410 nm (3.18 - 3.02 eV) of light wavelength, matching with the band edge of anatase (3.2 eV) and rutile (3.05 eV) phase of TiO₂. Reflectance spectra (Fig. 2.9, bottom) show an increase in reflectance while the transmittance spectra show a decrease in transmittance with increasing annealing temperature. This decrease in transmittance is partly due to higher reflectance and partly due to higher absorption at higher annealing temperature, as is observed with our SE results which shows increase in both n and k with annealing temperature.

To have an estimate of the optical energy gap, absorption coefficient (α) of the films, near the absorption edge, were calculated from the transmittance (T) and reflectance (R) data using the simplified relation $T=(1-R)e^{-\alpha d}$, where d is the thickness of the films. The intercept of the tangent to the $(\alpha h\nu)^{1/2}$ vs. $h\nu$ plot, where $h\nu$ is the photon energy, will give an estimate of the optical gap energy of a polycrystalline material. Plots of both $(\alpha h\nu)^{1/2}$ vs. $h\nu$ are drawn for the annealed films and are shown in Fig. 2.10. Optical gap energies obtained for amorphous TiO₂ (3.25 eV) is slightly higher than that of crystalline TiO₂ of anatase modification (3.15 eV) and are in close agreement with those reported in the literature [32]. However, for rutile modification of TiO₂, which is known to have an optical gap of around 3 eV [32], no linear relationship has been obtained in the $(\alpha h\nu)^{1/2}$ vs. $h\nu$ plot for our sample. This may be due to formation of some defect sites causing subband gap absorption and/or scattering (coherent) of light by relatively larger particles of this sample as can be seen from the SEM micrographs of Fig. 2.4.

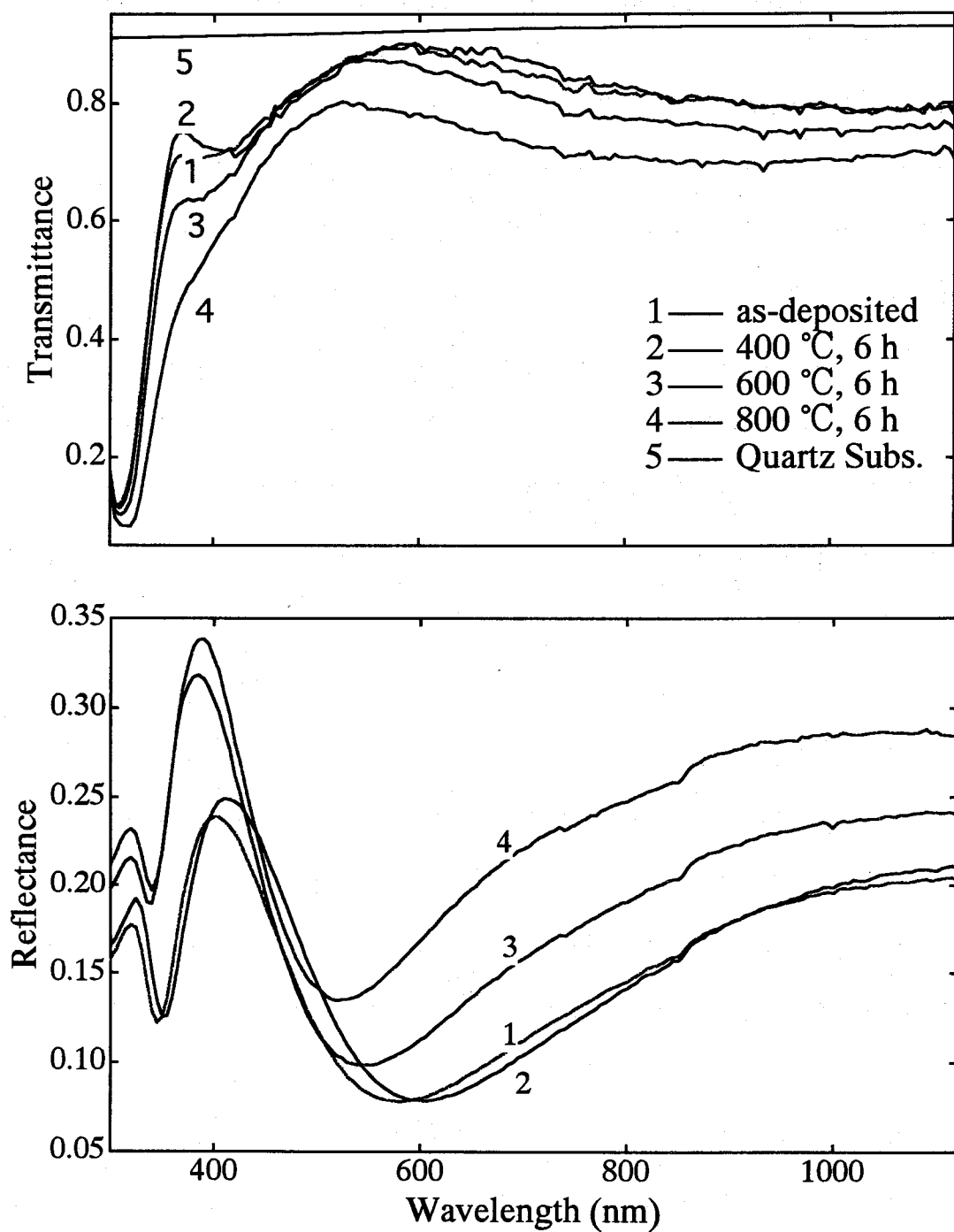


Fig. 2.9 Transmittance (top) and reflectance (bottom) spectra of TiO_2 thin films deposited on fused quartz substrate, annealed at different temperatures.

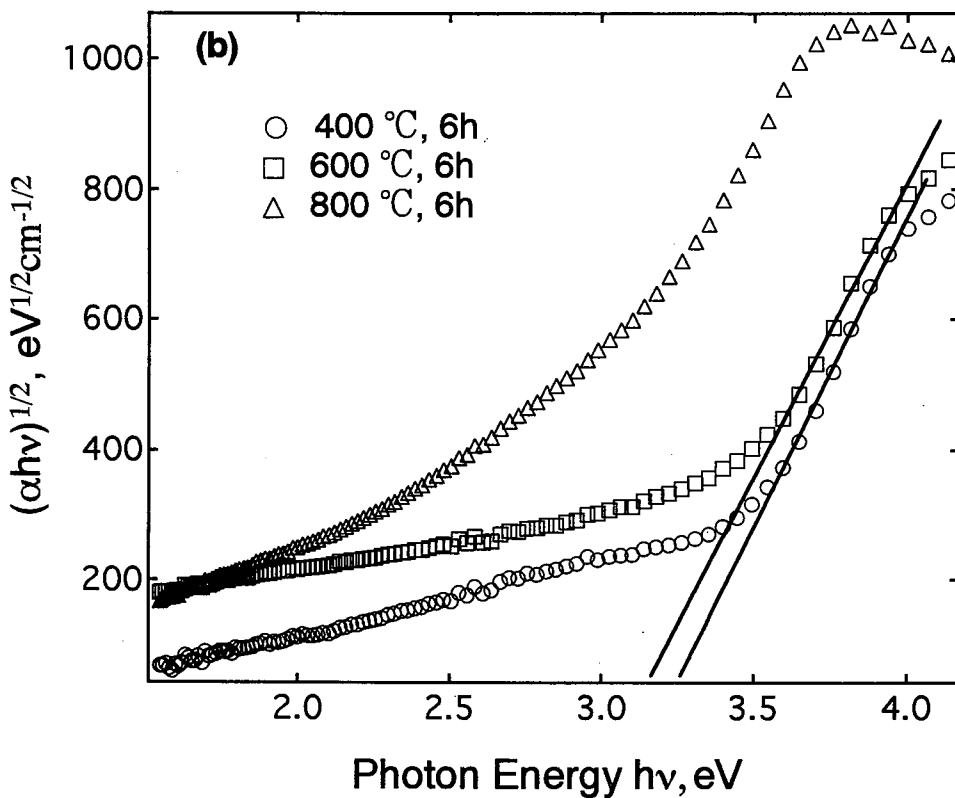


Fig. 2.10 Plots of $(\alpha h\nu)^{1/2}$ vs. $h\nu$ of TiO_2 thin films deposited on fused quartz substrate under different temperature conditions for the determination of optical energy gap.

2.3.2.3 Photoluminescence spectroscopy

Photoluminescence spectra of the films were recorded at different measurement temperatures using a 325 nm He-Cd laser source. An intense yellowish green photoluminescence is observed in the visible region with wide spectral width which is found to increase in intensity for higher temperature annealed samples. Figure 2.13 shows the room temperature (RT) PL spectrum of pure anatase TiO_2 thin film deposited on Si substrate at 600 °C. This spectrum resembles the luminescence spectrum of both single and polycrystalline TiO_2 reported by others [33,34]. The large difference between the band gap energy (~3.15 eV) and the emission peak energy (2.48 eV), which is around 0.67 eV, is described as the Stokes shift due to the Frank-Condon effect. The small peak at 3.06 eV, which is closer to the TiO_2 band gap energy, may be due to the near band gap emission. In the inset of Fig. 2.13 are shown

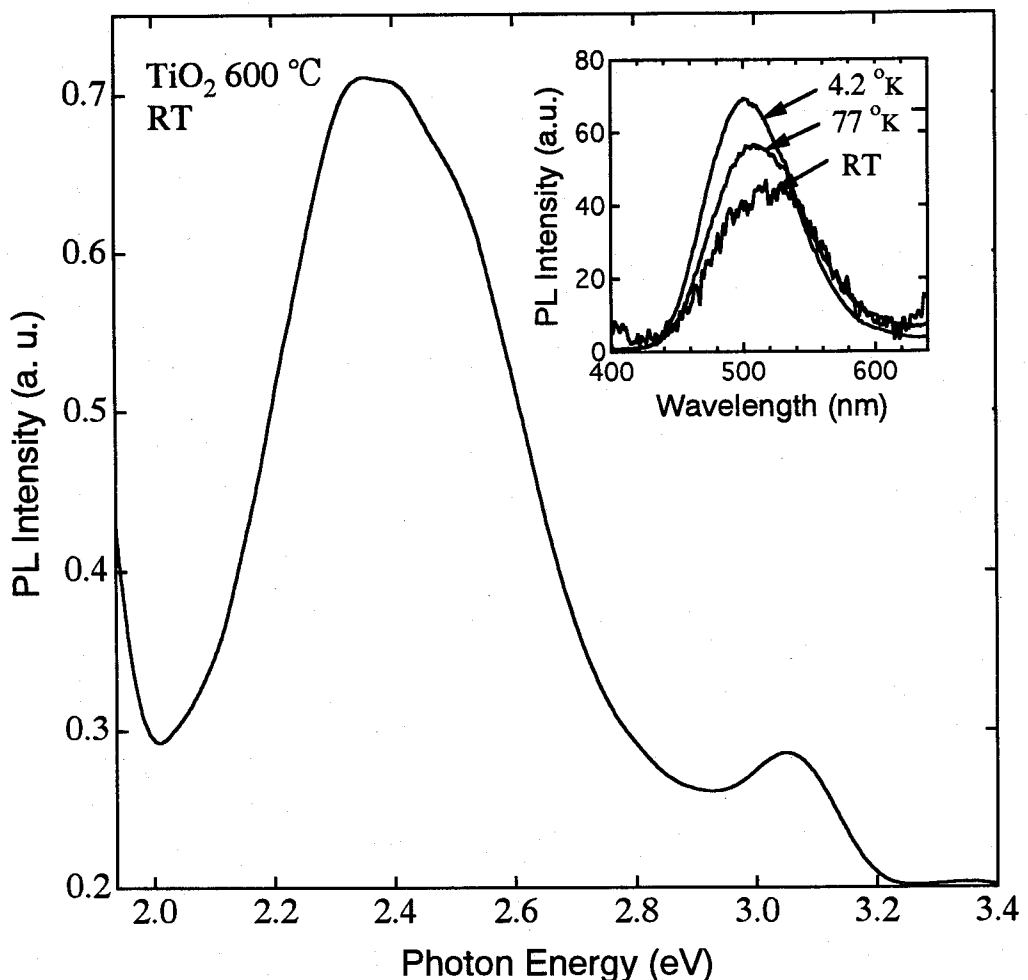


Fig. 2.11 Room temperature PL spectra of pure TiO₂ thin film, deposited on Si substrate, at 600 °C, by sol-gel process. Inset shows PL spectra of the same sample, measured at different temperatures.

the PL spectra of the same film measured at 4.2 K, 77 K and RT. As can be seen from this figure, at very low temperature (4.2 K), the spectrum is relatively sharp and smooth, while at higher temperatures the band becomes broad and the band peak shifts towards higher energies. The peak energies measured at 4.2 K, 77 K and RT are 2.41 eV, 2.43 eV and 2.46 eV, respectively, and the total shift is 0.05 eV.

2.3.3 Electrical

2.3.3.1 Conductivity study and effect of H₂ annealing

TiO₂ is a wide band gap semiconductor with very low conductivity. However, nano-pored nanocrystalline TiO₂ films are expected to have much higher resistivity because of large number of

trap sites and potential barriers at the grain boundaries. For conductivity measurement, films were deposited on both ITO coated glass and fused quartz substrates, and annealed at 600 °C for 1h which yields crystalline anatase TiO₂. Ohmic contact on the TiO₂ film was made with silver paste. *I – V* characteristics measured showed perfect ohmic nature of the silver contact with TiO₂ film. Conductivity study shows that conductivity across the film and along the film surface are around 10⁶ and 10⁹ ($\Omega \text{-cm}$)⁻¹, respectively. This directional dependence of conductivity can be understood from the fact that the nano-crystallites are more densely packed along the thickness of the film than they are along the plane of the film surface, as observed from the SEM cross-sectional (Fig. 2.5) and surface (Fig. 2.4) micrographs, which results in higher conductance along the thickness. One may anticipate that while measuring the conductivity across the film, silver particles from the electrode may penetrate into the pore of nano-crystalline TiO₂ and falsely show the increase in conductivity. In order to find out if there is any such effect, conductivity across the film was measured for two film thicknesses (one with 5 times coated and the other with 10 times coated) and almost same result was obtained for both the films which shows that this effect is negligible since in that case the thinner film would have shown higher conductivity than the thicker one.

Conductivity of TiO₂ can be increased by reducing it in vacuum, or in H₂ or CO/CO₂ atmosphere, which create donor levels near the conduction band [35]. The reduction is characterized by the loss of stoichiometry, i. e., TiO_{2-x}, in other words, formation of oxygen vacancy described as Ti³⁺ – V_O – Ti³⁺ [18], which can donate one or two electrons to the conduction band. Previous study revealed higher rate of TiO₂ reduction in H₂ atmosphere which has been explained by the rapid migration of atomic hydrogen into the bulk, and rapid diffusion of OH to the surface [36]. In effect oxygen vacancies diffuse rapidly into the bulk. We have studied the effect of reduction of TiO₂ films, by heat-treating in H₂ atmosphere, deposited on both the ITO coated glass and fused quartz substrates. The color of the films deposited on ITO coated glass substrate when annealed in H₂ atmosphere gradually changes from white to gray to dark brown with annealing time and the conductivity of the films increases greatly. However, the films deposited on quartz substrate remain

transparent with a slight increase in conductivity even after 1h of H_2 annealing. It is believed that for the films deposited on quartz substrate, some oxygen out diffusion from the substrate is taking place compensating the oxygen lost during H_2 annealing. Also, the effect of H_2 annealing on the photoconductivity has been studied and is shown in Fig. 2.12.

Upon irradiation with a solar simulator under 1 sun AM0 conditions, the as deposited films reveal photoconductivity in the range of 4-5 order of magnitude. Both the dark and photo-conductivity

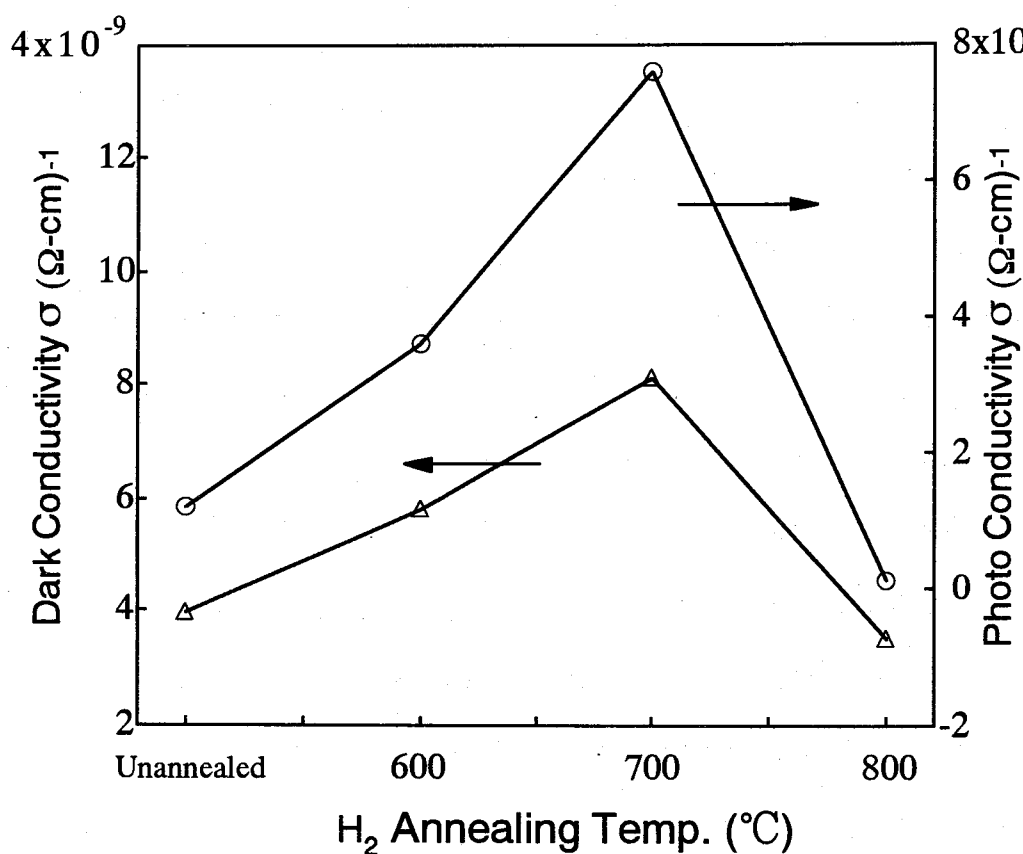


Fig. 2.12 Dark (Δ) and Photoconductivity (\circ) of as deposited and H_2 annealed TiO_2 thin films, deposited on fused quartz substrate.

increases upto 700 $^{\circ}C$ annealing temperature and thereafter the photo-conductivity decreases rapidly with a simultaneous decrease in dark conductivity. The increased conductivity at elevated temperature (upto 700 $^{\circ}C$) is attributed in part to the improved crystallinity, as observed by the X-ray diffraction patterns of the films (Fig. 2.13), and in part to the faster reduction rate at higher temperature. However, increase in annealing temperature above 700 $^{\circ}C$, which is a transition temperature of anatase phase to rutile, degrades the crystallinity as can be seen by the broadening in the X-ray peak

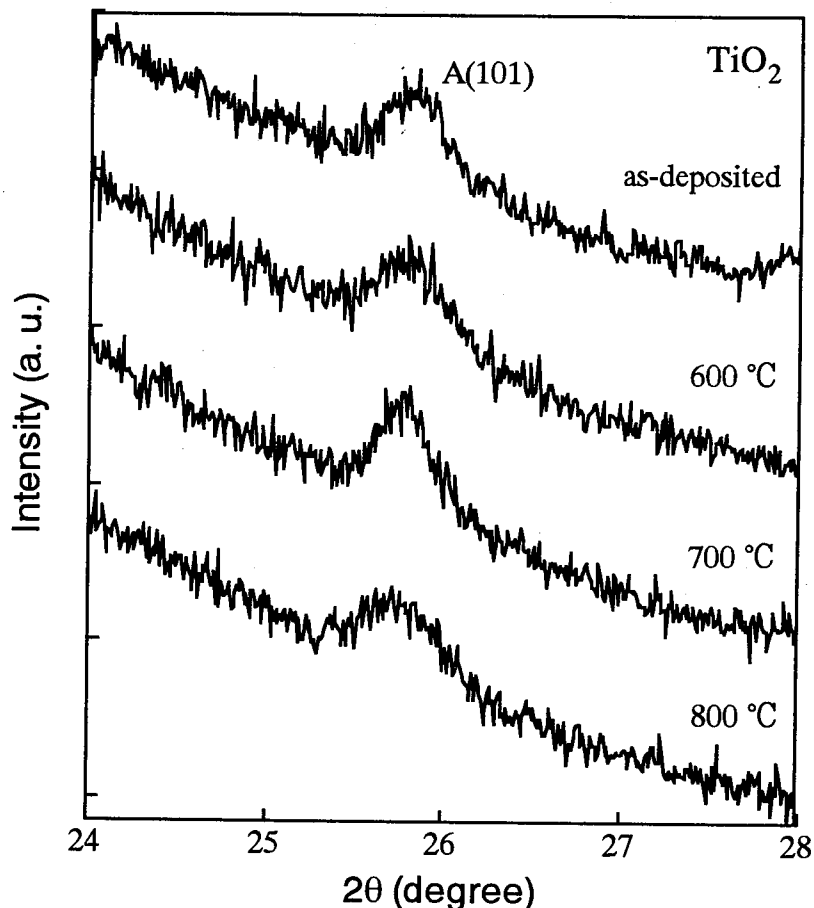


Fig. 2.13 X-ray diffraction patterns of as deposited and H_2 annealed TiO_2 thin films deposited on fused quartz substrate. (A: anatase)

(Fig. 2.13), and thus causes both the dark and photo-conductivity to decrease.

2.4 Conclusions

TiO_2 thin films have been deposited on single crystal silicon, sapphire and fused quartz substrates by sol-gel dip-coating method and annealed at different temperatures. Films deposited under same condition on different substrates show different structural properties. The as-deposited films on sapphire and silicon substrates are polycrystalline, anatase type, while that on the quartz substrate is amorphous in nature. Up to 600 °C annealing temperature, films are polycrystalline, single phase, anatase type for all the substrates, above which (800 °C) films are rutile (on quartz and

sapphire substrates) or a mixture of A/R (on Si substrate), depending upon substrate topography. Surface morphology by SEM reveals nanocrystalline porous structure of the films.

Spectroscopic ellipsometry results show increase in both n and k with increasing annealing temperature, may be due to the increase in crystallinity and phase transformation, as also observed by XRD patterns, and are in consistent with UV-visible spectroscopic measurements. Optical energy gaps estimated from UV-visible transmission and reflectance measurement are 3.25 and 3.15 eV for amorphous and anatase TiO₂, respectively. Conductivity study shows the nano-crystalline films to be highly resistive, in the range of $10^6\text{--}10^9 \Omega\text{-cm}$. Further, conductivity across the film has been found to be almost 3 order of magnitude higher than that along the surface of the film. Pure anatase films revealed good photoconductivity, of the order of 4 – 5, and both the dark and photo-conductivity increased upon annealing in H₂ atmosphere up to 700 °C annealing temperature.

References

- [1] K. Fukushima, I. Yamada and T. Takagi, *J. Appl. Phys.* **58** (1985) 4146.
- [2] M. Lottiaux, C. Boulesteix, G. Nihoul, F. Varnier, F. Flory, R. Galindo and E. Pelletier, *Thin Solid Films* **170** (1989) 107.
- [3] L. Ketron, *Bull. Am. Ceram. Soc.* **68** (1989) 860.
- [4] G. P. Burns, *J. Appl. Phys.* **65** (1989) 2095.
- [5] M. A. Fox and M. T. Dulay, *Chem. Rev.* **93** (1993) 341.
- [6] A. Fujishima and K. Honda, *Nature* **238** (1972) 37.
- [7] P. J. Boddy, *J. Electrochem. Soc.* **115** (1968) 119.
- [8] M. D. Archer, *J. Appl. Electrochem.* **5** (1975) 17.
- [9] B. O'Regan and M. Gratzel, *Nature* **353** (1991) 737.
- [10] T. Yoko, A. Yuasa, K. Kamiya and S. Sakka, *J. Electrochem. Soc.* **138** (1991) 2279.
- [11] A. Aoki and G. Nogami, *J. Electrochem. Soc.* **143** (1996) L191.
- [12] Y. Ha, S. W. Nam, T. H. Lim, I. H. Oh and S. A. Hong, *J. Membrane Sci.* **11** (1996) 81.
- [13] T. Oyama, Y. Iimura, K. Takeuchi and T. Ishii, *J. Mater. Sci. Let.* **15** (1996) 594.
- [14] H. Weller and A. Eychmuller, in *Semiconductor Nanoclusters - Physical, Chemical and Catalytic Aspects*, P. V. Kamat and D. Meisel (ed), Elsevier Science Publishers B. V., Amsterdam, The Netherlands, 1997, p. 5.
- [15] H. Hidaka, *J. Photochem., Photobiol. A : chem.* **109** (1997) 165.
- [16] L. L. Hench and D. R. Ulrich (eds), in *Ultrastructure Processing of Ceramics, Glasses and Composites*, Wiley-Interscience, New York, 1984.
- [17] F. A. Grant, *Rev. Mod. Phys.* **31** (1959) 646.
- [18] J. B. Goodenough, *Prog. Solid State Chem.* **5** (1971) 145.
- [19] V. E. Henrich, *Rep. Prog. Phys.* **48** (1985) 1481.
- [20] J. Yuan and S. Tsujikawa, *J. Electrochem. Soc.* **142** (1995) 3444.

- [21] D. E. Aspnes and A. A. Studna, *Phys. Rev.* **27** (1983) 985.
- [22] S. Y. Kim, *Appl. Opt.* **35** (1996) 6703.
- [23] T. Gerfin and M. Gratzel, *J. Appl. Phys.* **79** (1996) 1722.
- [24] J. A. Woollam, W. A. McGahan and B. Johs, *Thin Solid Films* **241** (1994) 44.
- [25] D. E. Aspnes, *Thin Solid Films* **89** (1982) 249.
- [26] K. Memarzadeh, J. A. Woollam and A. Belkind, *J. Appl. Phys.* **64** (1988) 3407.
- [27] W. H. Press, B. P. Flannery, S. A. Teukolsky and W. T. Vetterling, Numerical Recipes:
The art of Scientific Computing, Cambridge University Press, Cambridge, England, 523ff.
- [28] K. A. Vorotilov, E. V. Orlova and V. I. Petrovsky, *Thin Solid Films* **207** (1992) 180.
- [29] L. Ward, *The Optical Constants of Bulk Materials and Film*, 2nd ed, IOP Publishing Ltd,
Bristol, 1994, England, p. 20.
- [30] M. H. Suhail, G. M. Rao and S. Mohan, *J. Appl. Phys.* **71** (1992) 1421.
- [31] K. N. Rao, M. A. Murthy and S. Mohan *Thin Solid Films* **176** (1989) 181.
- [32] H. O. Finklea, in *Semiconductor Electrodes*, H. O. Finklea (ed), Elsevier Science
Publishers B. V., Amsterdam, The Netherlands, 1988, pp. 49-50, and references therein.
- [33] H. Tang, K. Prasad, R. Sanjines, P. E. Schmid and F. Levy, *J. Appl. Phys.* **75**, (1994) 2042.
- [34] H. Tang, H. Berger, P. E. Schmid, F. Levy and G. Burri, *Solid State Commun.* **87**,
(1993) 847.
- [35] H. O. Finklea, in *Semiconductor Electrodes*, H. O. Finklea (ed), Elsevier Science
Publishers B. V., Amsterdam, The Netherlands, 1988, p. 55.
- [36] J. B. Goodenough, A. Hamnet, M. P. Dare-Edwards, G. Campet and R. D. Wright,
Surf. Sci. **101** (1980) 531.